Continuous Hypoxia Reduces Retinal Ganglion Cell Degeneration in a Mouse Model of Mitochondrial Optic Neuropathy

Alexander M. Warwick,[1] Howard M. Bomze,[1,2] Luyu Wang,[1] Mikael Klingeborn,[1,*] Ying Hao,[1] Sandra S. Stinnett,[1] and Sidney M. Gospe III[1]

[1]Department of Ophthalmology, Duke University School of Medicine, Durham, North Carolina, United States
[2]Department of Pharmacology and Cancer Biology, Duke University School of Medicine, Durham, North Carolina, United States

Correspondence: Sidney M. Gospe III, Department of Ophthalmology, Duke University School of Medicine, Box 3712 Med Center, 2351 Erwin Road, Durham, NC 27710, USA; sid.gospe@duke.edu.

Current affiliation: *McLaughlin Research Institute, Great Falls, Montana, United States.

Received: September 20, 2022
Accepted: December 4, 2022
Published: December 20, 2022

Citation: Warwick AM, Bomze HM, Wang L, et al. Continuous hypoxia reduces retinal ganglion cell degeneration in a mouse model of mitochondrial optic neuropathy. *Invest Ophthalmol Vis Sci.* 2022;63(13):21. https://doi.org/10.1167/iovs.63.13.21

Purpose. To test whether continuous hypoxia is neuroprotective to retinal ganglion cells (RGCs) in a mouse model of mitochondrial optic neuropathy.

Methods. RGC degeneration was assessed in genetically modified mice in which the floxed gene for the complex I subunit NDUFS4 is deleted from RGCs using *Vlgut2*-driven Cre recombinase. Beginning at postnatal day 25 (P25), *Vglut2-Cre;ndufs4*$^{loxP/loxP}$ mice and control littermates were housed under hypoxia (11% oxygen) or kept under normoxia (21% oxygen). Survival of RGC somas and axons was assessed at P60 and P90 via histological analysis of retinal flatmounts and optic nerve cross-sections, respectively. Retinal tissue was also assessed for gliosis and neuroinflammation using western blot and immunofluorescence.

Results. Consistent with our previous characterization of this model, at least one-third of RGCs had degenerated by P60 in *Vglut2-Cre;ndufs4*$^{loxP/loxP}$ mice remaining under normoxia. However, continuous hypoxia resulted in complete rescue of RGC somas and axons at this time point, with normal axonal myelination observed on electron microscopy. Though only partial, hypoxia-mediated rescue of complex I–deficient RGC somas and axons remained significant at P90. Hypoxia prevented reactive gliosis at P60, but the retinal accumulation of Iba1^{+} mononuclear phagocytic cells was not substantially reduced.

Conclusions. Continuous hypoxia achieved dramatic rescue of early RGC degeneration in mice with severe mitochondrial dysfunction. Although complete rescue was not durable to P90, our observations suggest that investigating the mechanisms underlying hypoxia-mediated neuroprotection of RGCs may identify useful therapeutic strategies for optic neuropathies resulting from less profound mitochondrial impairment, such as Leber hereditary optic neuropathy.

Keywords: hypoxia, mitochondria, complex I, Leigh syndrome, Leber hereditary optic neuropathy, retinal ganglion cell

Mitochondrial dysfunction is an underlying contributor to a variety of optic neuropathies, some of which arise from heritable mutations.[1,2] The prime example of a mitochondrial optic neuropathy is Leber hereditary optic neuropathy (LHON), which is characterized by rapidly progressive, profound vision loss in both eyes due to degeneration of retinal ganglion cells (RGCs), manifesting most often in adolescents and young adults.[3] LHON is among the most common mitochondrial diseases, with a reported prevalence of 1:30,000 to 1:50,000.[4–6] With rare exception,[7,8] it is caused by mutations in the mitochondrial DNA (mtDNA), resulting in partial loss of function of mitochondrial complex I, a large protein complex localizing to the mitochondrial inner membrane that is responsible for entry of electrons from reduced nicotinamide adenine dinucleotide (NADH) into the electron transport chain. Complex I is composed of seven mtDNA-encoded subunits and at least 37 nuclear-encoded subunits.[9] Loss of complex I activity impairs the oxidative adenosine triphosphate–generating capacity of cells[10] and, perhaps even more importantly, results in the leakage of electrons and the formation of deleterious reactive oxygen species (ROS).[11]

LHON has been challenging to model in mammals due to the technical difficulty of manipulating the mitochondrial genome. Previously characterized animal models have involved *in vivo* delivery of mutant complex I genes to RGCs by adeno-associated virus or use of genetically modified mouse lines. These models have demonstrated RGC degeneration but with a latency of at least 6 months and in some cases 1 to 2 years, limiting their utility for rapid screening of potential therapeutic strategies.[12–15] We recently adapted a mouse model of Leigh syndrome, a severe systemic

mitochondrial disease, in order to develop a genetically modified mouse line with much more rapid RGC degeneration than is observed in these LHON models.[16] Deletion of the nuclear gene *ndufs4*, which encodes an accessory complex I subunit mutated in some forms of Leigh syndrome, severely destabilizes complex I and decreases its enzymatic activity by >50% in the retina and other tissues.[17–20] This severe compromise of complex I function produces a more profound phenotype than seen in LHON, with germline *ndufs4* knockout mice exhibiting a rapidly progressive myoencephalopathy that results in death by around postnatal day 50 (P50).[18] In order to generate a model of mitochondrial optic neuropathy in which RGC degeneration could be studied over a longer period, we used Cre recombinase driven by the vesicular glutamate transporter V-Glut2 to delete floxed *ndufs4* alleles from RGCs. With complex I dysfunction induced in all RGCs but in only a subset of central nervous system neurons, the *Vglut2-Cre;ndufs4*$^{loxP/loxP}$ conditional knockout mice survive nearly twice as long as germline knockouts and manifest a rapid degeneration of RGCs that begins ~P45 and progresses to the loss of more than half of RGCs by P90.[16] The onset of acute RGC loss just after the mice reach sexual maturity is similar to many human cases of LHON and supports the use of this mouse line as a preclinical model for the disease.

The germline *ndufs4*$^{-/-}$ mouse line has been very well studied in recent years, and several laboratories have reported pharmacological interventions that may prolong the lifespan of these mice.[21–25] Aside from gene therapy that restores *ndufs4* expression,[26,27] the most successful therapy described in this mouse model has been to rear the mutant mice under continuous normobaric hypoxia. Mootha and colleagues have reported that housing the mice at an 11% O_2 concentration results in prolongation of the median lifespan to 270 days while also reducing neurological dysfunction.[28,29] It has been proposed that reduction of the O_2 tension at the tissue level in this mouse model is critical to relieving the burden of ROS formation.[30]

It is clear that profound hypoxia (as may occur in the setting of vascular occlusions or global hypoperfusion of the central nervous system) may result in RGC degeneration and optic atrophy.[31,32] However, overt RGC injury was not observed in mice subjected to a more moderate level of hypoxia similar to that used in the studies by the Mootha laboratory.[33] Therefore, we were interested in exploring the potential therapeutic value of hypoxia in our model of RGC-specific *ndufs4* deletion. Here, we report that an 11% O_2 environment achieved a striking 100% rescue of RGC soma and axon degeneration at P60, along with a reduction of retinal gliosis. Although incomplete, therapeutic efficacy remained robust at P90, indicating that further exploration of the mechanisms underlying the hypoxia-mediated rescue of complex I–deficient RGCs may identify promising therapeutic targets for patients with mitochondrial optic neuropathies, including LHON.

Methods

Animals

All animal experiments adhered to the ARVO Statement for the Use of Animals in Ophthalmic and Vision Research, following a protocol approved by the Institutional Animal Care and Use Committee of Duke University. *Vglut2-Cre;ndufs4*$^{loxP/loxP}$ mice and control littermates were generated as previously described[16] and maintained on a C57Bl/6J background.

Continuous Hypoxia

For hypoxia experiments, mouse cages were kept within a hypoxia chamber (A-Chamber animal cage enclosure; BioSpherix, Ltd., Parish, NY, USA) that lowers the ambient PO_2 by pumping in nitrogen gas to displace the oxygen. The chamber PO_2 level was set to a constant 11% O_2. For all experiments, mice born under normoxia were placed into the hypoxia chamber at P25 and maintained there until P60 or P90, under a 12-hour light/dark cycle. Cages with control littermates were maintained on their rack under a normoxic 21% O_2 concentration. At the indicated time points, the mice were removed from the hypoxia chamber and rapidly euthanized, followed by tissue harvesting for histology.

Antibodies

The following antibodies were used for immunofluorescence experiments: rabbit polyclonal anti-RBPMS1 (1:500, NBP2-20112, lot #130-96; Novus Biologicals, Englewood, CO, USA), rabbit polyclonal anti-Iba1 (1:1000, 019–19741; Fujifilm Wako Chemicals Corporation, Richmond, VA, USA), and rabbit polyclonal anti-GFAP (D1F4Q) XP (1:200, lot #12389; Cell Signaling Technology, Danvers, MA, USA). For western blot analysis of retinal lysates, the rabbit polyclonal anti-GFAP (D1F4Q) XP antibody was used at a dilution of 1:1000, and mouse monoclonal anti-β-actin (1:1000, sc-47778, lot #D0615; Santa Cruz Biotechnology, Dallas, TX, USA) was used as a loading control. Secondary antibodies against the appropriate species conjugated to Invitrogen Alexa Fluor 488 (immunofluorescence experiments, 1:500 dilution) or Invitrogen Alexa Fluor 680 or 800 (western blot experiments, 1:20,000 dilution) were purchased from Thermo Fisher Scientific (Waltham, MA, USA). Cell nuclei were stained using Hoechst 33342 (1:1000; Thermo Fisher Scientific).

Histological Techniques

Immunohistochemistry experiments were performed as previously described.[16,34] Briefly, posterior eyecups obtained from euthanized mice were fixed for 1 hour in 4% paraformaldehyde. Retinal flatmounts were then prepared by isolating the retinas, blocking in 5% goat serum in PBS with 0.3% Triton X-100, incubating with anti-RBPMS1 primary antibody in block for 5 days at 4°C, and incubating with anti-rabbit Alexa Fluor 488 in block overnight at 4°C. The retinas were then washed and placed on glass slides with the RGC layer facing up, and four radial cuts were made from the edge to the equator of each retina to achieve flattening prior to mounting.

Retinal cryosections were prepared by cryoprotecting fixed eyecups in 30% sucrose and then embedding them in optimal cutting temperature medium (Tissue-Tek; Sakura Finetek USA, Torrance, CA, USA). Retinal cross-sections through the optic nerve head, 20 µm in thickness, were collected using a cryostat microtome (Microm HM550; Thermo Fisher Scientific). Sections were rehydrated with PBS, blocked in 5% goat serum in PBS with 0.3% Triton X-100, and then incubated in primary antibody in the same blocking solution overnight at 4°C. Sections were washed and incubated with appropriate secondary antibody

Investigative Ophthalmology & Visual Science

conjugated to Alexa Fluor 488 overnight at 4°C and were washed prior to mounting.

All samples were mounted with Epredia Immu-Mount (Thermo Fisher Scientific) under glass coverslips. Images were acquired using an ECLIPSE Ti2 inverted confocal microscope, a CFI Plan Fluor 60× (oil) objective, and an A1 confocal scanner controlled by NIS-Elements software (Nikon, Tokyo, Japan). For RGC soma quantification in retinal flatmounts, images 45,000 μm^2 in area were obtained in each quadrant at locations of 0.5, 1.0, and 1.5 mm from the optic nerve head, and RGC somas were manually counted using the Cell Counter plugin for Fiji.[35] RGC soma density was averaged among the four quadrants at each distance from the optic nerve head. For quantification of $Iba1^+$ cells, retinal cross-sections were imaged along their entire length, and the number of labeled cells within the ganglion cell and inner plexiform layers was quantified in three or four retinal sections per sample (taken through the optic nerve head), then averaged. For quantification of glial fibrillary acidic protein (GFAP)-positive radial processes of Müller glia, 45,000 μm^2 images were acquired at a 500-µm distance to either side of the optic nerve head for three sections per sample. The number of positive radial processes present at the inner nuclear layer/inner plexiform layer junction was counted for each section and averaged.

To assess RGC axons, mouse optic nerves were obtained from euthanized mice that had undergone transcardial perfusion with 4% paraformaldehyde and then post-fixed for an additional 2 hours in 2% paraformaldehyde and 2% glutaraldehyde in PBS. Samples were embedded in EMbed 812 resin mixture (Electron Microscopy Sciences, Hatfield, PA, USA) and sectioned on an ultramicrotome (LKB Ultratome V; Leica, Wetzlar, Germany) using a glass knife. Cross-sections of 0.27-µm thickness were stained with 1% methylene blue. Axon cross-section images were obtained using a Nikon ECLIPSE Ti2 microscope and NIS-Elements imaging software. For each optic nerve cross-section, four images obtained using a 60× (oil) objective were stitched in order to capture the entire nerve. This was performed on three cross-sections per optic nerve to ensure consistency. Axon count analysis was performed using the AxoNet plugin for ImageJ (National Institutes of Health, Bethesda, MD, USA).[36] The final axon count was averaged over the three cross-sections and then divided by the total optic nerve area to determine mean axon density per nerve.

The same mouse optic nerve specimens were thinly sectioned (60–80 nm) for transmission electron microscopy. Samples were collected on copper grids, counterstained with uranyl acetate and Sato's lead, and then examined using an electron microscope (JEM-1400; JEOL USA, Peabody, MA, USA) at 60 kV. Images were collected using an Orius charge-coupled device camera (Gatan, Pleasanton, CA, USA).

Western Blot for GFAP Quantification

To quantify GFAP protein abundance, freshly dissected retinas were sonicated in cOmplete Mini buffer (25-mM HEPES buffer, pH 7.4; 150-mM NaCl; 5-mM $MgCl_2$; and protease inhibitors; Roche, Indianapolis, IN, USA) with 1% Triton X-100. The protein concentration of each lysate was determined with a colorimetric assay (Bio-Rad, Hercules, CA, USA). After mixing with sodium dodecyl sulfate–polyacrylamide gel electrophoresis (SDS-PAGE) sample buffer, four retinal lysates from each experimental group were separated on 10% to 20% SDS-PAGE gels, transferred onto polyvinylidene fluoride membranes, and blotted with the indicated primary antibodies overnight. Membranes were washed in 0.05% Tween 20 and incubated with the appropriate secondary antibody for 2 hours. The Odyssey CLx imaging system (LI-COR Biosciences, Lincoln, NE, USA) was used to image and quantify band intensities. For each sample, the intensity of the GFAP band was normalized to that of the band for β-actin, which served as the loading control.

Experimental Design and Statistical Analysis

Histological assessment of RGC soma and axon survival was performed on *Vglut2-Cre;ndufs4*$^{loxP/loxP}$ and littermate control mice, with both sexes represented. In these experiments, eight to 14 retinas or optic nerves were analyzed for each genotype and O_2 concentration at each time point. Histological quantification of GFAP localization within Müller glia processes and $Iba1^+$ mononuclear cells in the inner retina was performed in four or five retinas for each genotype, O_2 concentration, and time point. In all quantitative histological analyses, the observer was masked to the identity of each sample. For all experiments, statistical comparisons between groups were made with the Wilcoxon rank-sum test to account for non-parametric data. All data analysis for this study was generated using SAS 9.4 for Windows (SAS Institute, Cary, NC, USA). Data are presented graphically as mean ± SEM.

Results

Hypoxia Achieves Complete Histological Rescue of RGCs in *Vglut2-Cre;ndufs4*$^{loxP/loxP}$ Mice at P60 and Remains Therapeutic at P90

We have previously observed that RGC somas and axons develop normally in *Vglut2-Cre;ndufs4*$^{loxP/loxP}$ mice, with no histological phenotype at P30 and only mild degeneration observed at P45.[16] Given the absence of early degeneration prior to weaning, we elected to initiate continuous hypoxia at P25. *Vglut2-Cre;ndufs4*$^{loxP/loxP}$ mice and control *ndufs4*$^{loxP/loxP}$ littermates lacking Cre recombinase were subjected to normoxia (21% O_2) or hypoxia (11% O_2) through P60. At this age, the conditional knockout mice did not manifest an overt neurological phenotype under either oxygen concentration, consistent with prior observations.[16,37] RGC soma density was assessed on retinal flatmounts stained with the RGC marker RBPMS1 (Fig. 1A). As we had observed previously, *Vglut2-Cre;ndufs4*$^{loxP/loxP}$ mice raised entirely under normoxia demonstrated a reduction of RGC density by approximately one third, and this was observed at locations proximal, intermediate, and distal from the optic nerve head ($P \leq 0.01$ for all locations) (Fig. 1B). In contrast, no degeneration of RGC somas was observed when mice were treated with hypoxia; the soma density was indistinguishable between *Vglut2-Cre;ndufs4*$^{loxP/loxP}$ housed at 11% O_2 from P25 to P60 and control *ndufs4*$^{loxP/loxP}$ mice exposed to either O_2 concentration.

To determine the durability of the hypoxia-mediated RGC rescue, additional cohorts of mice were analyzed at P90, the latest time point at which the normoxic *Vglut2-Cre;ndufs4*$^{loxP/loxP}$ mice could be assessed prior to death. At this time point, the conditional knockout mice maintained under normoxia were ataxic and manifested stiffness of the limbs, whereas those housed at 11% O_2 had a grossly

Investigative Ophthalmology & Visual Science

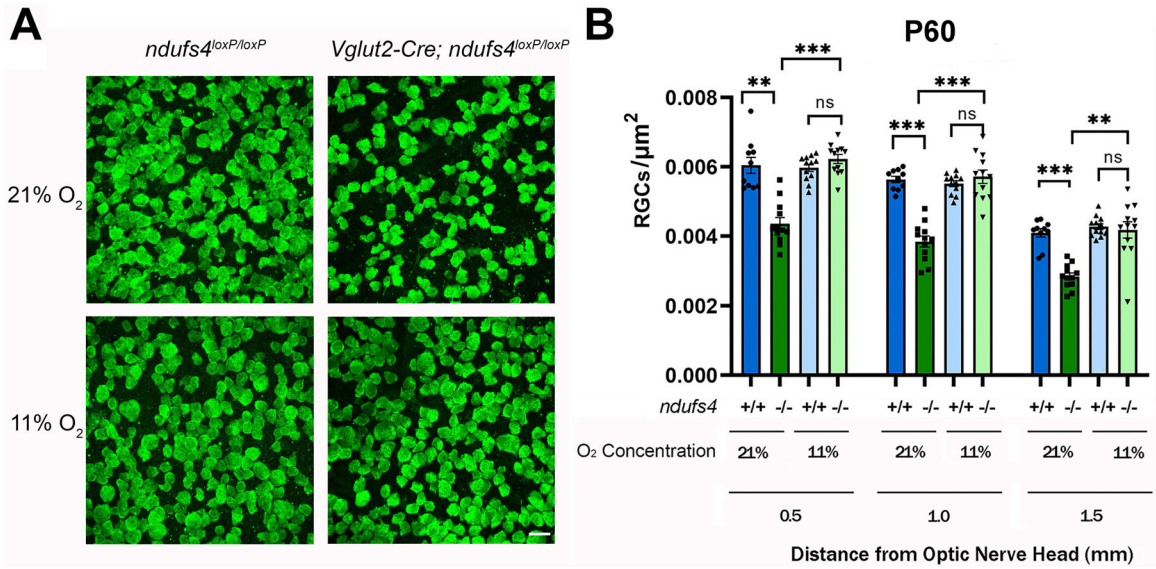

Figure 1. Continuous exposure to 11% O_2 prevents RGC soma degeneration at P60 in *Vglut2-Cre;ndufs4*$^{loxP/loxP}$ mice. (**A**) Representative images obtained from retinal flatmounts at locations 1.0 mm from the optic nerve head. RGC somas are immunolabeled with RNA-binding protein 1 (RBPMS1; *green*). Control *ndufs4*$^{loxP/loxP}$ mice lacking Cre recombinase (*left panels*) and conditional knockout *Vglut2-Cre;ndufs4*$^{loxP/loxP}$ mice (*right panels*) were housed under normoxic conditions (21% O_2; *top row*) or under hypoxia (11% O_2; *bottom row*) from P25 to P60. The reduction of RGC soma density in normoxic *Vglut2-Cre;ndufs4*$^{loxP/loxP}$ retinas at P60 was prevented by continuous hypoxia. *Scale bar*: 20 µm. (**B**) RGC soma density (RGC somas/µm^2) for the indicated genotypes and environmental O_2 concentrations are shown at three different distances from the optic nerve head: 0.5, 1.0, and 1.5 mm. *ndufs4*$^{+/+}$ indicates intact copies of both alleles (*ndufs4*$^{loxP/loxP}$ mice), whereas *ndufs4*$^{-/-}$ indicates deletion of both alleles (*Vglut2-Cre;ndufs4*$^{loxP/loxP}$ mice). Individual data points are depicted as *black circles*, *squares*, or *triangles*. Data are presented as mean ± SEM. Statistical comparisons between groups are indicated above the bars, with the following significance designations: ns, non-significant; $^{**}P \leq 0.01$; $^{***}P \leq 0.001$.

normal systemic phenotype. Further RGC loss of approximately 45% was observed in *Vglut2-Cre;ndufs4*$^{loxP/loxP}$ mice raised entirely under normoxia (Figs. 2A, 2B). In contrast to the earlier time point of P60, the rescue of RGC degeneration by hypoxia was no longer complete at P90; however, the extent of RGC soma loss was reduced by >50% at all three locations within the retina ($P < 0.01$ for all). In this experiment, cohorts of heterozygous *Vglut2-Cre;ndufs4*$^{loxP/+}$ mice were also included in order to verify that the loss of only one copy of *ndufs4* in RGCs is aphenotypic and that the expression of Cre recombinase itself had no effect on our analyses. Consistent with prior reports of a normal systemic phenotype in heterozygous germline *ndufs4*$^{+/-}$ mice,[30] we observed that RGC soma density was completely normal at P90 regardless of the ambient O_2 concentration, confirming that this genotype may serve as a useful control in subsequent experiments, as it allows for more efficient breeding of experimental mice.

Continuous Hypoxia Reduces Axonal Degeneration in *Vglut2-Cre;ndufs4*$^{loxP/loxP}$ Mice

As a complementary assessment of the neuroprotective effect of hypoxia on RGCs from *Vglut2-Cre;ndufs4*$^{loxP/loxP}$ mice, optic nerve cross-sections were obtained in order to quantify RGC axon density and to assess for morphological rescue. At P60, axon density was reduced by 58% in the optic nerves of normoxic *Vglut2-Cre;ndufs4*$^{loxP/loxP}$ mice compared to *Vglut2-Cre;ndufs4*$^{loxP/+}$ control mice, whereas the axon density was significantly increased in the knockouts raised under hypoxia ($P < 0.001$) and no different from the controls (Figs. 3A, 3B). Electron microscopy revealed reduced axon density with increased surrounding fibrosis and abnormal myelination patterns in the optic nerves of normoxic *Vglut2-Cre;ndufs4*$^{loxP/loxP}$ mice (Fig. 3C). In contrast, an orderly, healthy appearance of myelinated RGC axons was observed in hypoxic *Vglut2-Cre;ndufs4*$^{loxP/loxP}$ mice, indistinguishable from that of control littermates.

Consistent with our analysis of RGC somas, a partial rescue of RGC axons was apparent at P90. Although the hypoxia-treated *Vglut2-Cre;ndufs4*$^{loxP/loxP}$ mice exhibited a 32% reduction in axon density compared to control mice, this represented a rescue of 45% of the axons lost under normoxic conditions (Figs. 4A, 4B). Ultrastructural analysis of the optic nerves via electron microscopy demonstrated the interim development of abnormal myelination patterns in the hypoxia-raised *Vglut2-Cre;ndufs4*$^{loxP/loxP}$ mice at P90 compared to the P60 time point; however, the morphological abnormalities were demonstrably less severe than in the cohort kept continuously under normoxia (Fig. 4C).

Hypoxia Reduces Reactive Gliosis Without Significantly Mitigating Neuroinflammation in *Vglut2-Cre;ndufs4*$^{loxP/loxP}$ Retinas

Neuroinflammation—an accumulation of mononuclear phagocytic cells within brain lesions, often in conjunction with surrounding glial cell activation—is a key pathological feature of *ndufs4* knockout mice and has been observed to be prevented or decreased by interventions that extend the lifespan and reduce neurological dysfunction in these mice.[21,29,38,39] Notably, retinal gliosis and inner retinal accumulation of Iba1$^+$ mononuclear cells have been observed to accompany RGC degeneration in both the germline

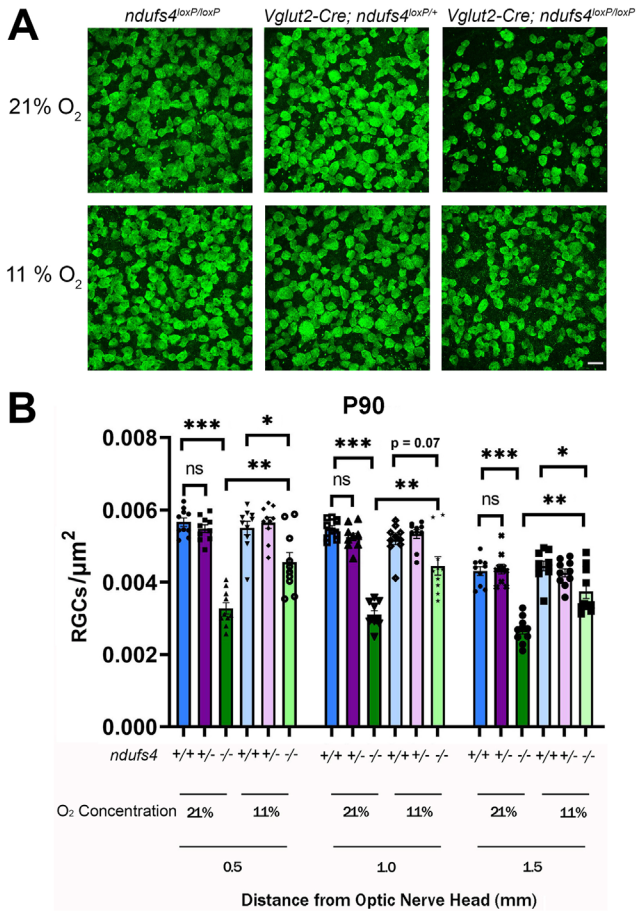

Figure 2. RGC soma degeneration in *Vglut2-Cre;ndufs4*$^{loxP/loxP}$ mice is partially rescued by hypoxia at P90. (A) Representative images obtained from retinal flatmounts at locations 1.0 mm from the optic nerve head. RGC somas are immunolabeled with RBPMS1 (*green*). Control *ndufs4*$^{loxP/loxP}$ mice lacking Cre recombinase (*left panels*), *Vglut2-Cre;ndufs4*$^{loxP/+}$ mice with only one allele of *ndufs4* deleted by Cre (*middle panels*), and *Vglut2-Cre;ndufs4*$^{loxP/loxP}$ mice with both alleles of *ndufs4* deleted (*right panels*) were housed under normoxic conditions (21% O_2; *top row*) or under hypoxia (11% O_2; *bottom row*) from P25 to P90. Only with deletion of both copies of *ndufs4* was RGC soma degeneration observed at P90, and this level of degeneration was markedly reduced by continuous hypoxia. *Scale bar*: 20 µm. (**B**) RGC soma density (RGC somas/µm^2) for the indicated genotypes and environmental O_2 concentrations are shown at three different distances from the optic nerve head: 0.5, 1.0, and 1.5 mm. *ndufs4*$^{+/+}$ indicates intact copies of both alleles (*ndufs4*$^{loxP/loxP}$ mice; *blue bars*), *ndufs4*$^{+/-}$ indicates deletion of one allele of *ndufs4* (*Vglut2-Cre;ndufs4*$^{loxP/+}$ mice; *purple bars*), and *ndufs4*$^{-/-}$ indicates deletion of both alleles (*Vglut2-Cre;ndufs4*$^{loxP/loxP}$ mice; *green bars*). Individual data points are overlaid on each bar. Statistical comparisons between groups are indicated above the bars, with the following significance designations: ns, non-significant; $^{*}P \leq 0.05$; $^{**}P \leq 0.01$; $^{***}P \leq 0.001$.

ndufs4$^{-/-}$ mouse[40] and in our *Vglut2-Cre;ndufs4*$^{loxP/loxP}$ conditional knockout mouse line.[16] Given the neuroprotective effect of hypoxia on *ndufs4*-deficient RGCs, we wondered whether continuous hypoxia would produce a similar reduction of these abnormal histological findings in *Vglut2-Cre;ndufs4*$^{loxP/loxP}$ mice. As before, the *Vglut2-Cre;ndufs4*$^{loxP/loxP}$ mice and control *Vglut2-Cre;ndufs4*$^{loxP/+}$ littermates were exposed to either 21% O_2 or 11% O_2 from P25 until harvesting of ocular tissue at P60 or P90. Reactive gliosis was determined by assessing for upregulation of GFAP, an intermediate filament expressed constitutively by retinal astrocytes and detectable in Müller glia as a response to retinal pathology.[41–43] At P60, the abundance of GFAP protein was increased in the retinas of *Vglut2-Cre;ndufs4*$^{loxP/loxP}$ mice raised under normoxia by fourfold compared to *Vglut2-Cre;ndufs4*$^{loxP/+}$ controls ($P < 0.05$), whereas the retinal GFAP protein level in hypoxic *Vglut2-Cre;ndufs4*$^{loxP/loxP}$ mice was not increased (Fig. 5A). Compared to control *Vglut2-Cre;ndufs4*$^{loxP/+}$ mice, the inner retinal astrocytes of normoxic *Vglut2-Cre;ndufs4*$^{loxP/loxP}$ mice were thickened and exhibited bright immunolabeling for GFAP, which was also upregulated within the radial processes of Müller glia as a sign of retinal stress (Fig. 5B). In contrast, GFAP expression within Müller radial processes was prevented in *Vglut2-Cre;ndufs4*$^{loxP/loxP}$ mice raised under hypoxia at P60 ($P < 0.05$) (Fig. 5B). Similar to the partial hypoxia-mediated rescue of RGC somas seen at P90, the upregulation of GFAP was not completely prevented at this time point but was reduced by twofold ($P < 0.05$) (Fig. 5C). The number of GFAP-positive Müller radial processes was also intermediate in P90 *Vglut2-Cre;ndufs4*$^{loxP/loxP}$ mice treated with hypoxia compared to controls and *Vglut2-Cre;ndufs4*$^{loxP/loxP}$ mice raised under normoxia (Fig. 5D).

The effect of hypoxia on inner retinal Iba1^{+} mononuclear cell accumulation in *Vglut2-Cre;ndufs4*$^{loxP/loxP}$ mice was much less pronounced. As we previously observed,[16] there was a greater than twofold increase in Iba1^{+} cell abundance in P60 *Vglut2-Cre;ndufs4*$^{loxP/loxP}$ retinas under normoxia compared to controls; however, an intermediate abundance was observed at this early time point in mutant mice raised under hypoxia that was not significantly lower than in mice raised under normoxia (Fig. 5E). By P90, the accrual of mononuclear cells in the inner retina in *Vglut2-Cre;ndufs4*$^{loxP/loxP}$ mice was identical regardless of O_2 concentration. Thus, any effect of hypoxia on mononuclear phagocytic cell accumulation in the vicinity of complex I–deficient RGCs was modest at best, and in fact this buildup may be anticipatory to overt RGC death.

Discussion

In this study, we have shown that continuous hypoxia is neuroprotective when applied prior to the onset of RGC degeneration in mice with RGC-specific deletion of *ndufs4*. With hypoxia treatment, no discernible loss of RGC somas or axons was observed at P60, a time point at which approximately one third of RGCs have degenerated in *Vglut2-Cre;ndufs4*$^{loxP/loxP}$ mice raised entirely under normoxia. Compared to the systemic phenotypes of germline *ndufs4*$^{-/-}$ mice (e.g., ataxia, stiffness, inactivity, weight loss, early death), which have been reported to be delayed by a half year or more by hypoxia,[28,29] the therapeutic effect on optic atrophy in *Vglut2-Cre;ndufs4*$^{loxP/loxP}$ mice is less durable, as the 100% rescue of RGCs observed at P60 diminished to approximately 50% after 1 additional month, with accompanying signs of reactive gliosis by astrocytes and Müller cells. This more moderate reduction of optic atrophy by hypoxia is perhaps not surprising in light of the exquisite sensitivity of RGCs to chronic complex I dysfunction: in the setting of the milder insults to complex I function associated with LHON, most patients develop optic atrophy in the absence of other neurological or systemic symptoms.[44] In this context, the time-limited therapeutic effect of hypoxia on *ndufs4*-deficient RGCs may still hold significant

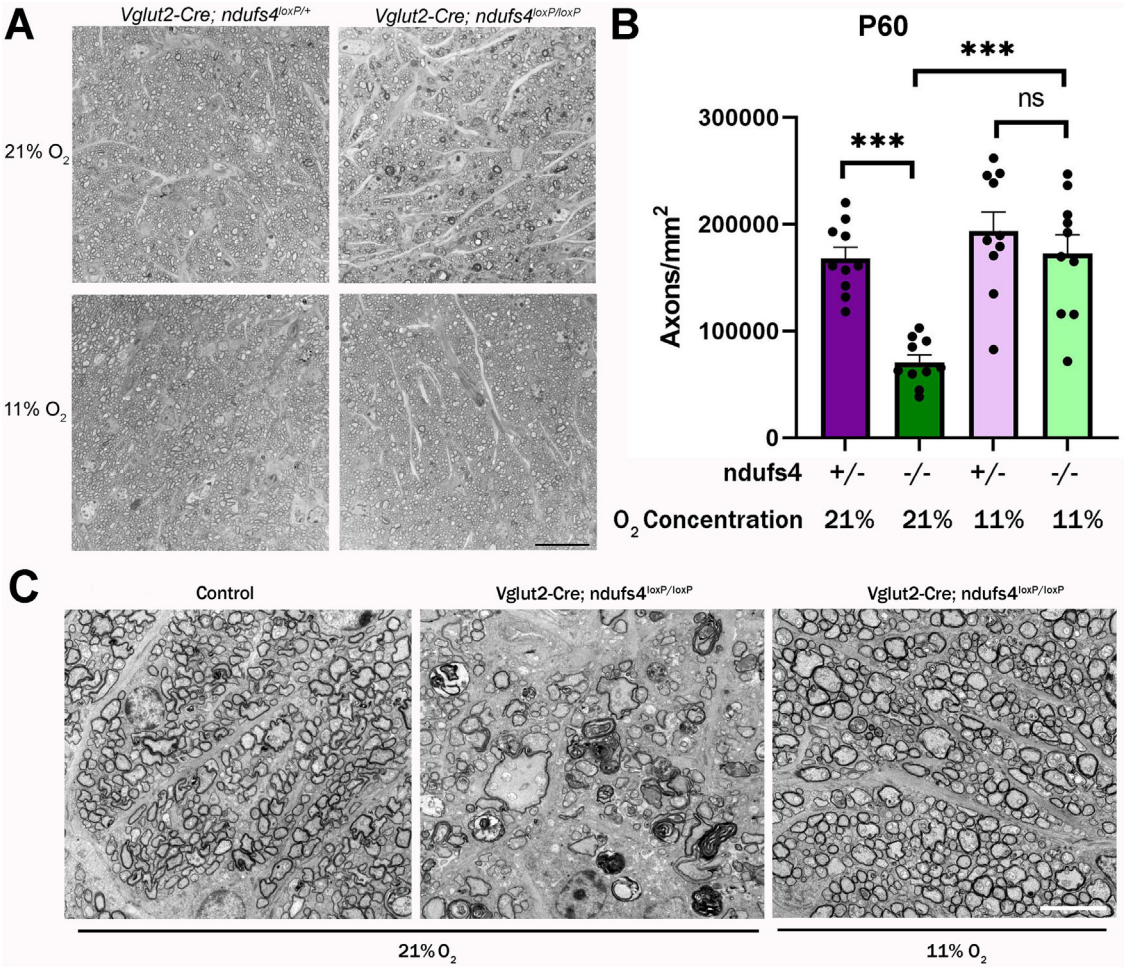

Figure 3. RGC axonal degeneration in *Vglut2-Cre;ndufs4*$^{loxP/loxP}$ mice at P60 is prevented by continuous hypoxia. (**A**) Representative light micrographs of optic nerve cross-sections stained with methylene blue. Control *Vglut2-Cre;ndufs4*$^{loxP/+}$ mice (*left column*) and conditional knockout *Vglut2-Cre;ndufs4*$^{loxP/loxP}$ mice (*right column*) were housed under normoxia (21% O_2, *upper row*) or hypoxia (11% O_2, *lower row*) from P25 to P60. *Scale bar*: 20 µm. (**B**) RGC axon densities in optic nerve cross-sections determined using AxoNet automated axon quantification. *ndufs4*$^{+/-}$ indicates deletion of one allele of *ndufs4* (*Vglut2-Cre;ndufs4*$^{loxP/+}$ mice; *purple bars*), and *ndufs4*$^{-/-}$ indicates deletion of both alleles (*Vglut2-Cre;ndufs4*$^{loxP/loxP}$ mice; *green bars*). The O_2 concentration is indicated for each group. Individual data points are depicted as *black circles*. Data are presented as mean ± SEM. Statistical comparisons between groups are indicated above the bars, with the following significance designations: ns, non-significant; $^{***}P \leq 0.001$. (**C**) Electron micrographs (5000×) of optic nerve cross-sections at P60 demonstrate preservation of normal axon morphology and abundance in *Vglut2-Cre;ndufs4*$^{loxP/loxP}$ mice raised under continuous hypoxia (*right*) compared to normoxia (*middle*). *Scale bar*: 5 µm.

relevance to developing treatments for LHON, as hypoxia might offer a more sustained neuroprotection of RGCs with milder complex I dysfunction. An important next step, therefore, would be to conduct a long-term assessment of the effect of hypoxia on the more slowly developing optic neuropathies characteristic of mouse models with LHON-associated mutations in complex I subunits.[12,13]

A key future direction will be to elucidate the mechanisms underlying the salutary effect of hypoxia on complex I–deficient RGCs, as this may facilitate the development of targeted pharmacological interventions that could protect RGCs with mitochondrial impairment while potentially obviating the need for direct hypoxia. Among a number of possible mechanisms that could underpin hypoxia-mediated RGC neuroprotection is the reprogramming of cellular bioenergetics away from oxidative metabolism and in favor of non-oxidative metabolic pathways such as glycolysis. Notably, the hypoxia-inducible factor (HIF) pathway—the primary driver of many cellular adaptions in response to hypoxia—upregulates expression of the glucose transporter Glut1 and a number of glycolytic enzymes among its many transcriptional targets.[45,46] However, Mootha and colleagues recently reported that constitutive activation of the HIF pathway under normoxia could not substitute for hypoxia in extending the lifespan of germline *ndufs4*$^{-/-}$ mice.[30] Thus, although the necessity of the HIF pathway in the hypoxia-mediated rescue of severe complex I dysfunction has not been directly tested, HIF activation by itself is clearly not sufficient.

An alternative—but not necessarily mutually exclusive—therapeutic mechanism is a hypoxia-mediated reduction of oxidative stress within complex I–deficient cells. Complex I dysfunction impairs the passage of NADH-derived electrons to ubiquinone and to subsequent complexes of the electron transport chain, instead increasing the likelihood of electron leakage from complex I and a consequent production

Investigative Ophthalmology & Visual Science

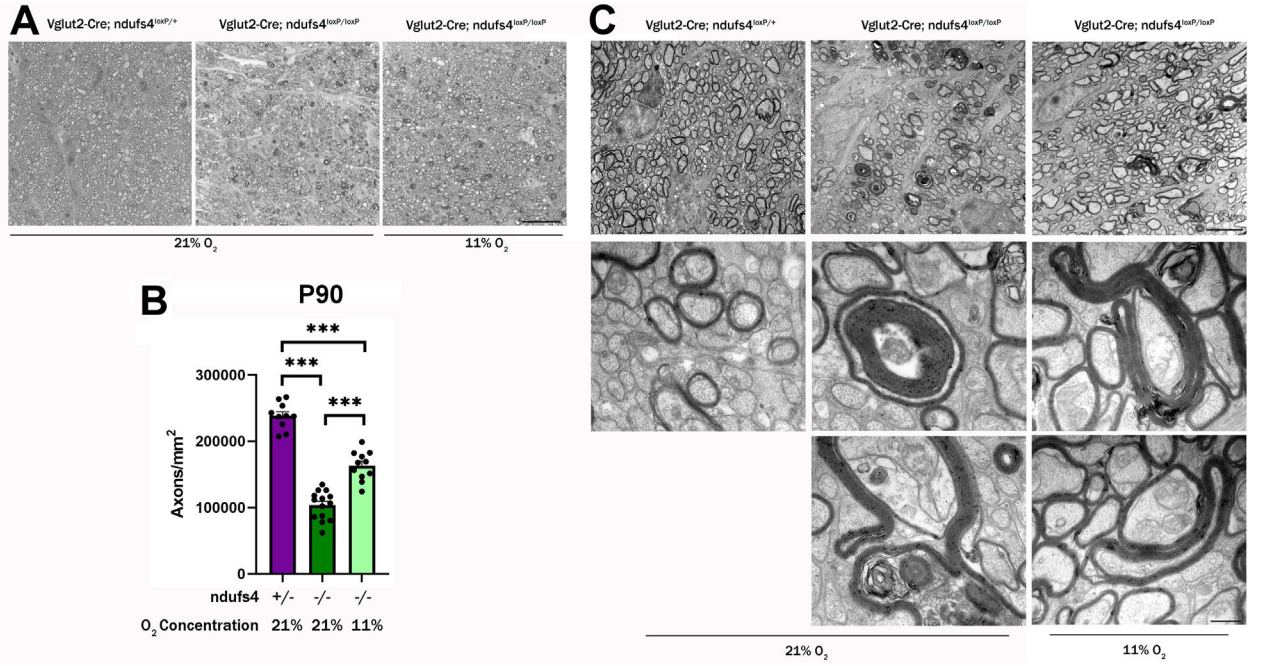

Figure 4. Retinal ganglion cell axonal degeneration is reduced in P90 *Vglut2-Cre;ndufs4*$^{loxP/loxP}$ mice treated with hypoxia. (**A**) Representative light micrographs of optic nerve cross-sections stained with methylene blue for *Vglut2-Cre;ndufs4*$^{loxP/+}$ control mice kept under normoxia (21% O_2, *left*), *Vglut2-Cre;ndufs4*$^{loxP/loxP}$ mice kept under normoxia (*middle*), and *Vglut2-Cre;ndufs4*$^{loxP/loxP}$ mice treated with hypoxia (11% O_2, *right*) from P25 to P90. *Scale bar*: 20 µm. (**B**) RGC axon densities in optic nerve cross-sections at P90 determined using AxoNet automated axon quantification. *ndufs4*$^{+/-}$ indicates deletion of one allele of *ndufs4* (*Vglut2-Cre;ndufs4*$^{loxP/+}$ mice; *purple bar*), and *ndufs4*$^{-/-}$ indicates deletion of both alleles (*Vglut2-Cre;ndufs4*$^{loxP/loxP}$ mice; *green bars*). The O_2 concentration is indicated for each group. Individual data points are depicted as *black circles*. Data are presented as mean ± SEM. Statistical comparisons between groups are indicated above the bars. $^{***}P \leq 0.001$. (**C**) Electron micrographs with magnifications of 5000× (*top row*; *scale bar*: 5 µm) and 40,000× (*bottom two rows*; *scale bar*: 0.5 µm) demonstrate axon density and morphology in P90 optic nerve cross-sections from normoxic *Vglut2-Cre;ndufs4*$^{loxP/+}$ control mice (*left column*) and *Vglut2-Cre;ndufs4*$^{loxP/loxP}$ mice kept under normoxia (*middle column*) or hypoxia (*right column*). The higher magnification images demonstrate typical abnormalities in myelination that occur in *Vglut2-Cre;ndufs4*$^{loxP/loxP}$ optic nerves, including thickening and doubling of the myelin sheaths and incomplete enclosure of axons. Although these abnormalities may be observed in hypoxia-treated animals (*right*), they are less frequent and generally less severe.

of deleterious ROS.[47] Moreover, as highlighted by Mootha and colleagues, the impairment of oxidative phosphorylation may result in an accumulation of unused O_2 in affected tissues, further favoring the formation of ROS. By limiting the availability of molecular oxygen, environmental hypoxia might thereby reduce the formation of ROS from electron leakage at a dysfunctional complex I. Supporting this concept, *in vivo* experiments in germline *ndufs4*$^{-/-}$ mice have indicated that impaired O_2 utilization within the brain results in relative hyperoxia at the tissue level; the neurologic improvement achieved when these mice are exposed to a hypoxic environment occurs in association with a restoration of brain tissue O_2 tension to normal levels.[30,48] However, although the "excess O_2" hypothesis is quite intuitive, it should be noted that, in other model systems, hypoxia itself has been shown to stimulate ROS formation.[49,50] Furthermore, unlike in the germline *ndufs4*$^{-/-}$ mouse, only ~1% to 2% of retinal neurons (the RGCs and a small minority of cones and horizontal cells) in our conditional knockout model have complex I impairment;[16] with the remainder of the retina retaining normal oxidative phosphorylation capacity, a significant accumulation of unused O_2 at the tissue level would seem unlikely.

Another potential neuroprotective mechanism that is particularly intriguing is the possibility that hypoxia could lead to enhanced mitochondrial biogenesis. Because the accumulation of oxidative damage to mitochondrial DNA and other macromolecules may lead to progressive metabolic dysfunction as part of the pathogenesis of mitochondrial diseases,[51] increasing the relative abundance of healthier new mitochondria might help to mitigate the effects of mitochondrial dysfunction. Indeed, there have been reports that individuals with higher mitochondrial DNA copy numbers (a proxy for mitochondrial abundance) may be relatively protected from vision loss in LHON.[52,53] Notably, cellular exposure to hypoxia in several model systems has been associated with upregulation of the mitochondrial biogenesis regulator peroxisome proliferator-activated receptor gamma coactivator 1-alpha (PGC-1α), and the resulting increase in mitochondrial biogenesis may occur as a HIF-independent process.[54–56]

Finally, the role of retinal neuroinflammation is important to consider in the context of hypoxia. At P60, when RGC degeneration and reactive gliosis of astrocytes and Müller cells in *Vglut2-Cre;ndufs4*$^{loxP/loxP}$ retinas were entirely suppressed by hypoxia, we nevertheless observed a trend toward an increase in Iba1$^+$ mononuclear cell abundance in the inner retina. By P90, the accumulation of Iba1$^+$ cells was not suppressed by hypoxia at all, despite a continued reduction of RGC degeneration. As the complex I deficiency in this mouse model is essentially limited to RGCs, it seems likely that the increase in mononuclear cells in the inner retinas of the *Vglut2-Cre;ndufs4*$^{loxP/loxP}$ mice occurs as a result of signals released by RGCs experiencing cellular

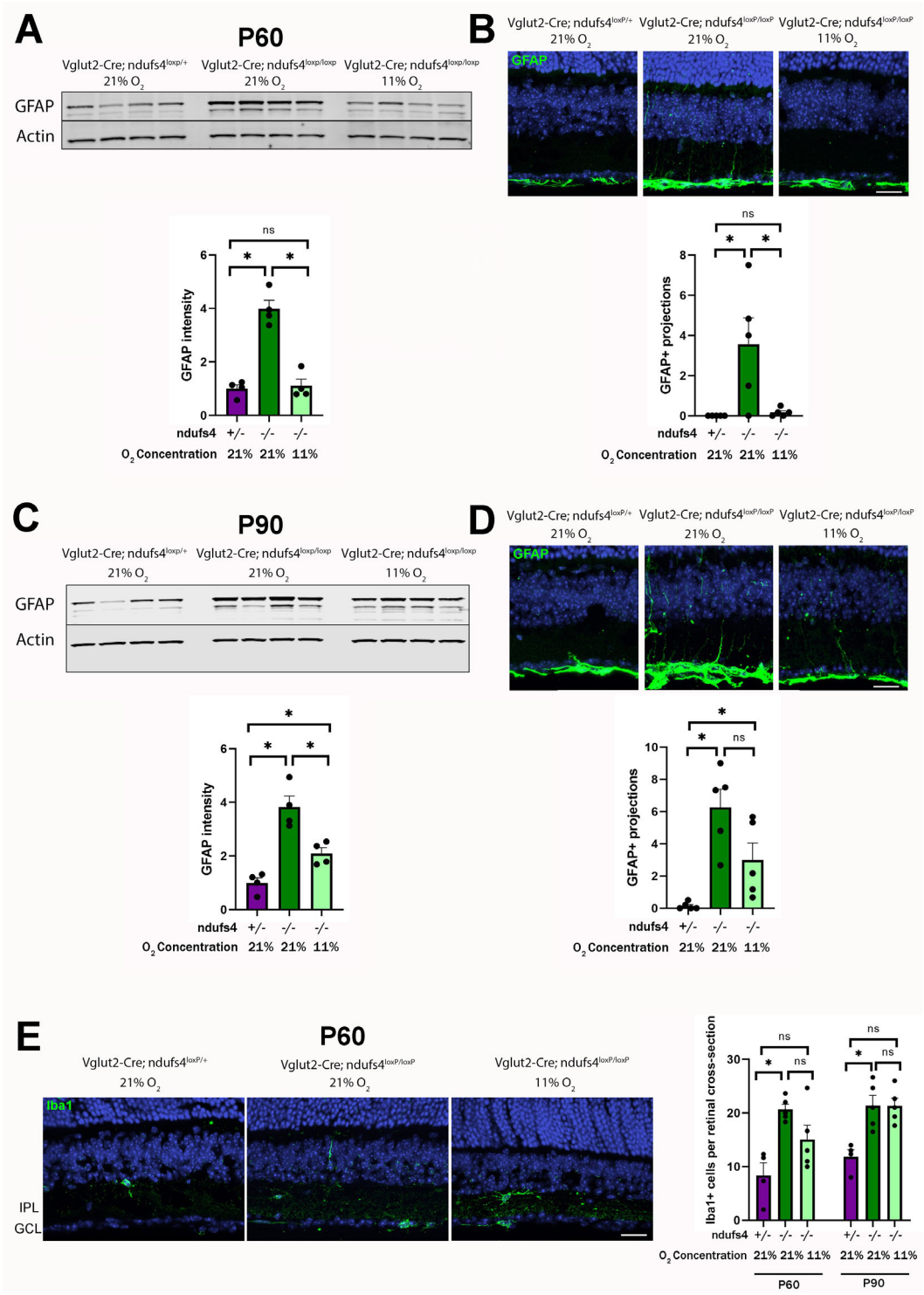

Figure 5. The effect of continuous hypoxia on retinal gliosis and neuroinflammation in *Vglut2-Cre;ndufs4*$^{loxP/loxP}$ mice. (**A**) GFAP expression levels in P60 retinal lysates assessed by western blot, with four replicates each for normoxic control *Vglut2-Cre;ndufs4*$^{loxP/+}$ mice (*left*) and for *Vglut2-Cre;ndufs4*$^{loxP/loxP}$ mice exposed to normoxia (middle) or hypoxia (*right*). The graph below depicts the relative increase in GFAP band intensity normalized to the actin compared to the control group. (**B**) Representative images of P60 retinal cross-sections immunolabeled with GFAP (*green*). In control *Vglut2-Cre;ndufs4*$^{loxP/+}$ mice (*left*), GFAP signal is present only in astrocytes of the inner-most retina, whereas in normoxic *Vglut2-Cre;ndufs4*$^{loxP/loxP}$ mice (*middle*), GFAP-positive radial projections of Müller glia are observed. This reactive gliosis is prevented by treating the mice with hypoxia (*right*). The graph below depicts the mean number of GFAP-positive Müller projections identified per 100-µm segment of retina for each group. (**C**) Western blot assessment of GFAP protein levels in retinal lysates at P90. As in **A**, the normalized GFAP band intensity is plotted relative to control. (**D**) Representative images of retinal cross-sections immunolabeled with GFAP (*green*) at P90 for the same experimental groups depicted in **B**. The abundance of GFAP-positive radial Müller projections is depicted in the graph below. (**E**) P60 retinal cross-sections were labeled with Iba1 (*green*) to identify mononuclear inflammatory cells. *Scale bar*: 20 µm. The mean number of Iba1^{+} cells within the ganglion cell layer (GCL) or inner plexiform layer (IPL) across a retinal section are depicted in the graph to the right for retinas obtained at P60 and P90. For all graphs, bars depict mean ± SEM, with individual data points displayed; ns, not significant; $^{*}P < 0.05$. Uncropped western blot images are available as supplementary material (Supplementary Fig. S1).

Investigative Ophthalmology & Visual Science

stress, even prior to the onset of overt cell death. This notion is supported by a previous global gene expression analysis of germline *ndufs4*$^{-/-}$ mouse retinas conducted at the early time point of P33, which identified inflammatory and immune-related pathways to be the most highly upregulated compared to control retinas.[40]

The accumulation of Iba1^{+} mononuclear cells as a manifestation of retinal neuroinflammation may represent an expansion of the resident retinal microglial population and/or an infiltration of peripheral monocytes.[57] In this setting, distinguishing microglia from monocytes based on immunophenotyping and morphological analysis can be challenging and may require more advanced techniques such as single-cell transcriptomics or *in vivo* lineage tracing.[58,59] Although an accrual of these mononuclear phagocytes and their production of cytokines frequently contribute to neurodegeneration,[60,61] there are some contexts in which activation of microglia is believed to have neuroprotective effects via removal of cellular debris and secretion of anti-inflammatory mediators.[58,62,63] Likewise, the exuberant reactive gliosis that often accompanies neuroinflammation may have consequences that are complex, with the potential for both neurodegenerative and neuroprotective effects.[63,64] Interestingly, despite the finding of a hypoxia-mediated reduction of Iba1^{+} cell accumulation in *ndufs4*$^{-/-}$ mouse brain lesions by Mootha and colleagues[29] and our finding of reduced retinal gliosis, other models have demonstrated that hypoxia itself may stimulate a pro-inflammatory microglial response and the activation of astrocytes and Müller glia.[33,61,65–67] These discrepancies might reflect different effects of short-term (hours or days) versus long-term hypoxia (months, as in our study) or of intermittent rather than continuous exposure to hypoxia.

Along these lines, we should note that two recent studies reported that treatment of germline *ndufs4*$^{-/-}$ mice with the colony stimulating factor-1 receptor (CSF1R) inhibitor pexidartinib resulted not only in depletion of Iba1^{+} mononuclear cells but also in suppression of brain lesion formation, reduction of neurological dysfunction, and prolongation of the lifespan of the mice.[39,68] These findings suggest that combatting inflammation can be neuroprotective in the setting of complex I dysfunction. Future studies in our mouse model testing whether the combination of anti-inflammatory interventions with hypoxia may result in additive or even synergistic RGC neuroprotection would therefore be very interesting.

In summary, we have demonstrated robust *in vivo* neuroprotection of complex I–deficient RGCs by continuous exposure to hypoxia. Our observations indicate that identifying the relevant cellular processes modulated by hypoxia may represent a critical step in addressing the unmet need of developing effective therapies for mitochondrial optic neuropathies such as LHON.

Acknowledgments

The authors thank Daniel Saban and Vadim Arshavsky for helpful discussions and critical review of the manuscript.

Supported by a grant from the National Eye Institute, National Institutes of Health (EY028610 to SMG); Core Grant EY005722 (Duke University); a Duke University School of Medicine Strong Start Award (SMG); a Career Development Award from Research to Prevent Blindness (SMG); and an unrestricted Research to Prevent Blindness grant to the Duke Eye Center.

Disclosure: **A.M. Warwick**, None; **H.M. Bomze**, None; **L. Wang**, None; **M. Klingeborn**, None; **Y. Hao**, None; **S.S. Stinnett**, None; **S.M. Gospe III**, None

References

1. Kamel K, Farrell M, O'Brien C. Mitochondrial dysfunction in ocular disease: focus on glaucoma. *Mitochondrion.* 2017;35:44–53.
2. Yu-Wai-Man P, Newman NJ. Inherited eye-related disorders due to mitochondrial dysfunction. *Hum Mol Genet.* 2017;26:R12–R20.
3. Wallace DC, Lott MT. Leber hereditary optic neuropathy: exemplar of an mtDNA disease. *Handb Exp Pharmacol.* 2017;240:339–376.
4. Gorman GS, Schaefer AM, Ng Y, et al. Prevalence of nuclear and mitochondrial DNA mutations related to adult mitochondrial disease. *Ann Neurol.* 2015;77:753–759.
5. Rosenberg T, Norby S, Schwartz M, et al. Prevalence and genetics of Leber hereditary optic neuropathy in the Danish population. *Invest Ophthalmol Vis Sci.* 2016;57:1370–1375.
6. Yu-Wai-Man P, Griffiths PG, Brown DT, Howell N, Turnbull DM, Chinnery PF. The epidemiology of Leber hereditary optic neuropathy in the north east of England. *Am J Hum Genet.* 2003;72:333–339.
7. Mansukhani SA, Mehta DG, Renaud DL, Whealy MA, Chen JJ, Bhatti MT. Nuclear DNA mutation causing a phenotypic Leber hereditary optic neuropathy plus. *Ophthalmology.* 2021;128:628–631.
8. Stenton SL, Sheremet NL, Catarino CB, et al. Impaired complex I repair causes recessive Leber's hereditary optic neuropathy. *J Clin Invest.* 2021;131:e138267.
9. Wirth C, Brandt U, Hunte C, Zickermann V. Structure and function of mitochondrial complex I. *Biochim Biophys Acta.* 2016;1857:902–914.
10. Baracca A, Solaini G, Sgarbi G, et al. Severe impairment of complex I-driven adenosine triphosphate synthesis in Leber hereditary optic neuropathy cybrids. *Arch Neurol.* 2005;62:730–736.
11. Bahr T, Welburn K, Donnelly J, Bai Y. Emerging model systems and treatment approaches for Leber's hereditary optic neuropathy: challenges and opportunities. *Biochim Biophys Acta Mol Basis Dis.* 2020;1866:165743.
12. Lin CS, Sharpley MS, Fan W, et al. Mouse mtDNA mutant model of Leber hereditary optic neuropathy. *Proc Natl Acad Sci USA.* 2012;109:20065–20070.
13. Yu H, Koilkonda RD, Chou TH, et al. Consequences of zygote injection and germline transfer of mutant human mitochondrial DNA in mice. *Proc Natl Acad Sci USA.* 2015;112:E5689–E5698.
14. Yu H, Sant DW, Wang G, Guy J. Mitochondrial transfer of the mutant human *ND6T14484C* gene causes visual loss and optic neuropathy. *Transl Vis Sci Technol.* 2020;9:1.
15. Qi X, Sun L, Lewin AS, Hauswirth WW, Guy J. The mutant human ND4 subunit of complex I induces optic neuropathy in the mouse. *Invest Ophthalmol Vis Sci.* 2007;48:1–10.
16. Wang L, Klingeborn M, Travis AM, Hao Y, Arshavsky VY, Gospe SM. Progressive optic atrophy in a retinal ganglion cell-specific mouse model of complex I deficiency. *Sci Rep.* 2020;10:16326.
17. Lake NJ, Compton AG, Rahman S, Thorburn DR. Leigh syndrome: one disorder, more than 75 monogenic causes. *Ann Neurol.* 2016;79:190–203.
18. Kruse SE, Watt WC, Marcinek DJ, Kapur RP, Schenkman KA, Palmiter RD. Mice with mitochondrial complex I deficiency develop a fatal encephalomyopathy. *Cell Metab.* 2008;7:312–320.

19. Quintana A, Kruse SE, Kapur RP, Sanz E, Palmiter RD. Complex I deficiency due to loss of Ndufs4 in the brain results in progressive encephalopathy resembling Leigh syndrome. *Proc Natl Acad Sci USA.* 2010;107:10996–11001.
20. Song L, Yu A, Murray K, Cortopassi G. Bipolar cell reduction precedes retinal ganglion neuron loss in a complex 1 knockout mouse model. *Brain Res.* 2017;1657:232–244.
21. Johnson SC, Yanos ME, Kayser EB, et al. mTOR inhibition alleviates mitochondrial disease in a mouse model of Leigh syndrome. *Science.* 2013;342:1524–1528.
22. Lee CF, Caudal A, Abell L, Nagana Gowda GA, Tian R. Targeting NAD^+ metabolism as interventions for mitochondrial disease. *Sci Rep.* 2019;9:3073.
23. Frambach S, van de Wal MAE, van den Broek PHH, et al. Effects of clofibrate and KH176 on life span and motor function in mitochondrial complex I-deficient mice. *Biochim Biophys Acta Mol Basis Dis.* 2020;1866:165727.
24. Lyu J, Zhao Y, Zhang N, et al. Bezafibrate rescues mitochondrial encephalopathy in mice via induction of daily torpor and hypometabolic state. *Neurotherapeutics.* 2022;19:994–1006.
25. Perry EA, Bennett CF, Luo C, et al. Tetracyclines promote survival and fitness in mitochondrial disease models. *Nat Metab.* 2021;3:33–42.
26. Liu S, Fu S, Wang G, et al. Glycerol-3-phosphate biosynthesis regenerates cytosolic NAD^+ to alleviate mitochondrial disease. *Cell Metab.* 2021;33:1974.e9–1987.e9.
27. Reynaud-Dulaurier R, Benegiamo G, Marrocco E, et al. Gene replacement therapy provides benefit in an adult mouse model of Leigh syndrome. *Brain.* 2020;143:1686–1696.
28. Ferrari M, Jain IH, Goldberger O, et al. Hypoxia treatment reverses neurodegenerative disease in a mouse model of Leigh syndrome. *Proc Natl Acad Sci USA.* 2017;114:E4241–E4250.
29. Jain IH, Zazzeron L, Goli R, et al. Hypoxia as a therapy for mitochondrial disease. *Science.* 2016;352:54–61.
30. Jain IH, Zazzeron L, Goldberger O, et al. Leigh syndrome mouse model can be rescued by interventions that normalize brain hyperoxia, but not HIF activation. *Cell Metab.* 2019;30:824.e3–832.e3.
31. Grego L, Pignatto S, Busolini E, et al. Spectral-domain OCT changes in retina and optic nerve in children with hypoxic-ischaemic encephalopathy. *Graefes Arch Clin Exp Ophthalmol.* 2021;259:1343–1355.
32. Kaur C, Foulds WS, Ling EA. Hypoxia-ischemia and retinal ganglion cell damage. *Clin Ophthalmol.* 2008;2:879–889.
33. Mesentier-Louro LA, Shariati MA, Dalal R, et al. Systemic hypoxia led to little retinal neuronal loss and dramatic optic nerve glial response. *Exp Eye Res.* 2020;193:107957.
34. Gospe SM, Travis AM, Kolesnikov AV, et al. Photoreceptors in a mouse model of Leigh syndrome are capable of normal light-evoked signaling. *J Biol Chem.* 2019;294:12432–12443.
35. Schindelin J, Arganda-Carreras I, Frise E, et al. Fiji: an open-source platform for biological-image analysis. *Nat Methods.* 2012;9:676–682.
36. Ritch MD, Hannon BG, Read AT, et al. Axonet: a deep learning-based tool to count retinal ganglion cell axons. *Sci Rep.* 2020;10:8034.
37. Bolea I, Gella A, Sanz E, et al. Defined neuronal populations drive fatal phenotype in a mouse model of Leigh syndrome. *eLife.* 2019;8:e47163.
38. McElroy GS, Reczek CR, Reyfman PA, Mithal DS, Horbinski CM, Chandel NS. NAD+ regeneration rescues lifespan, but not ataxia, in a mouse model of brain mitochondrial complex I dysfunction. *Cell Metab.* 2020;32:301–308.e6.
39. Stokes JC, Bornstein RL, James K, et al. Leukocytes mediate disease pathogenesis in the Ndufs4(KO) mouse model of Leigh syndrome. *JCI Insight.* 2022;7:e156522.
40. Yu AK, Song L, Murray KD, et al. Mitochondrial complex I deficiency leads to inflammation and retinal ganglion cell death in the Ndufs4 mouse. *Hum Mol Genet.* 2015;24:2848–2860.
41. Cuenca N, Fernandez-Sanchez L, Campello L, et al. Cellular responses following retinal injuries and therapeutic approaches for neurodegenerative diseases. *Prog Retin Eye Res.* 2014;43:17–75.
42. de Hoz R, Rojas B, Ramirez AI, et al. Retinal macroglial responses in health and disease. *Biomed Res Int.* 2016;2016:2954721.
43. Mac Nair CE, Schlamp CL, Montgomery AD, Shestopalov VI, Nickells RW. Retinal glial responses to optic nerve crush are attenuated in *Bax*-deficient mice and modulated by purinergic signaling pathways. *J Neuroinflammation.* 2016;13:93.
44. Newman NJ. Hereditary optic neuropathies: from the mitochondria to the optic nerve. *Am J Ophthalmol.* 2005;140:517–523.
45. Albadari N, Deng S, Li W. The transcriptional factors HIF-1 and HIF-2 and their novel inhibitors in cancer therapy. *Expert Opin Drug Discov.* 2019;14:667–682.
46. Hu CJ, Wang LY, Chodosh LA, Keith B, Simon MC. Differential roles of hypoxia-inducible factor 1α (HIF-1α) and HIF-2α in hypoxic gene regulation. *Mol Cell Biol.* 2003;23:9361–9374.
47. Wong A, Cavelier L, Collins-Schramm HE, et al. Differentiation-specific effects of LHON mutations introduced into neuronal NT2 cells. *Hum Mol Genet.* 2002;11:431–438.
48. Grange RMH, Sharma R, Shah H, et al. Hypoxia ameliorates brain hyperoxia and NAD^+ deficiency in a murine model of Leigh syndrome. *Mol Genet Metab.* 2021;133:83–93.
49. Solaini G, Baracca A, Lenaz G, Sgarbi G. Hypoxia and mitochondrial oxidative metabolism. *Biochim Biophys Acta.* 2010;1797:1171–1177.
50. Sulkshane P, Ram J, Thakur A, Reis N, Kleifeld O, Glickman MH. Ubiquitination and receptor-mediated mitophagy converge to eliminate oxidation-damaged mitochondria during hypoxia. *Redox Biol.* 2021;45:102047.
51. Wallace DC, Fan W. The pathophysiology of mitochondrial disease as modeled in the mouse. *Genes Dev.* 2009;23:1714–1736.
52. Bianco A, Martinez-Romero I, Bisceglia L, et al. Mitochondrial DNA copy number differentiates the Leber's hereditary optic neuropathy affected individuals from the unaffected mutation carriers. *Brain.* 2016;139:e1.
53. Giordano C, Iommarini L, Giordano L, et al. Efficient mitochondrial biogenesis drives incomplete penetrance in Leber's hereditary optic neuropathy. *Brain.* 2014;137:335–353.
54. Arany Z, Foo SY, Ma Y, et al. HIF-independent regulation of VEGF and angiogenesis by the transcriptional coactivator PGC-1α. *Nature.* 2008;451:1008–1012.
55. LaGory EL, Wu C, Taniguchi CM, et al. Suppression of PGC-1α is critical for reprogramming oxidative metabolism in renal cell carcinoma. *Cell Rep.* 2015;12:116–127.
56. Shoag J, Arany Z. Regulation of hypoxia-inducible genes by PGC-1α. *Arterioscler Thromb Vasc Biol.* 2010;30:662–666.
57. Reyes NJ, O'Koren EG, Saban DR. New insights into mononuclear phagocyte biology from the visual system. *Nat Rev Immunol.* 2017;17:322–332.
58. O'Koren EG, Yu C, Klingeborn M, et al. Microglial function is distinct in different anatomical locations during retinal homeostasis and degeneration. *Immunity.* 2019;50:723.e7–737.e7.
59. Reyes NJ, Mathew R, Saban DR. Fate mapping in vivo to distinguish bona fide microglia versus recruited

Investigative Ophthalmology & Visual Science

monocyte-derived macrophages in retinal disease. *Methods Mol Biol.* 2019;1834:153–164.

60. DiSabato DJ, Quan N, Godbout JP. Neuroinflammation: the devil is in the details. *J Neurochem.* 2016;139(suppl 2):136–153.
61. Kiernan EA, Smith SM, Mitchell GS, Watters JJ. Mechanisms of microglial activation in models of inflammation and hypoxia: implications for chronic intermittent hypoxia. *J Physiol.* 2016;594:1563–1577.
62. Chen Z, Trapp BD. Microglia and neuroprotection. *J Neurochem.* 2016;136(suppl 1):10–17.
63. Li Q, Barres BA. Microglia and macrophages in brain homeostasis and disease. *Nat Rev Immunol.* 2018;18:225–242.
64. Bringmann A, Iandiev I, Pannicke T, et al. Cellular signaling and factors involved in Müller cell gliosis: neuroprotective and detrimental effects. *Prog Retin Eye Res.* 2009;28:423–451.
65. Subirada PV, Vaglienti MV, Joray MB, Paz MC, Barcelona PF, Sanchez MC. Rapamycin and resveratrol modulate the gliotic and pro-angiogenic response in Müller glial cells under hypoxia. *Front Cell Dev Biol.* 2022;10:855178.
66. Aviles-Reyes RX, Angelo MF, Villarreal A, Rios H, Lazarowski A, Ramos AJ. Intermittent hypoxia during sleep induces reactive gliosis and limited neuronal death in rats: implications for sleep apnea. *J Neurochem.* 2010;112:854–869.
67. Tadmouri A, Champagnat J, Morin-Surun MP. Activation of microglia and astrocytes in the nucleus tractus solitarius during ventilatory acclimatization to 10% hypoxia in unanesthetized mice. *J Neurosci Res.* 2014;92:627–633.
68. Aguilar K, Comes G, Canal C, Quintana A, Sanz E, Hidalgo J. Microglial response promotes neurodegeneration in the Ndufs4 KO mouse model of Leigh syndrome. *Glia.* 2022;70:2032–2044.

Investigative Ophthalmology & Visual Science